

## Article

# Highly Efficient and Eco-Friendly Thermal-Neutron-Shielding Materials Based on Recycled High-Density Polyethylene and Gadolinium Oxide Composites

Donruedee Toyen<sup>1,2</sup>, Ekachai Wimolmala<sup>3</sup>, Kasinee Hemvichian<sup>4</sup> , Pattra Lertsarawut<sup>4</sup>   
and Kiadtisak Saenboonruang<sup>2,5,6,\*</sup> 

- <sup>1</sup> Department of Materials Science, Faculty of Science, Kasetsart University, Bangkok 10900, Thailand; donruedee.toyen@ku.th
  - <sup>2</sup> Special Research Unit of Radiation Technology for Advanced Materials (RTAM), Faculty of Science, Kasetsart University, Bangkok 10900, Thailand
  - <sup>3</sup> Polymer Processing and Flow (P-PROF) Research Group, Division of Materials Technology, School of Energy, Environment and Materials, King Mongkut's University of Technology Thonburi, Bangkok 10140, Thailand; ekachai.wim@kmutt.ac.th
  - <sup>4</sup> Nuclear Technology Research and Development Center, Thailand Institute of Nuclear Technology (Public Organization), Nakhon Nayok 26120, Thailand; kasinee@tint.or.th (K.H.); pattra@tint.or.th (P.L.)
  - <sup>5</sup> Department of Applied Radiation and Isotopes, Faculty of Science, Kasetsart University, Bangkok 10900, Thailand
  - <sup>6</sup> Specialized Center of Rubber and Polymer Materials in Agriculture and Industry (RPM), Faculty of Science, Kasetsart University, Bangkok 10900, Thailand
- \* Correspondence: kiadtisak.s@ku.th; Tel.: +66-2-562-5555 (ext. 646219)

**Abstract:** Due to the increasing demands for improved radiation safety and the growing concerns regarding the excessive use of plastics, this work aimed to develop effective and eco-friendly thermal-neutron-shielding materials based on recycled high-density polyethylene (r-HDPE) composites containing varying surface-treated gadolinium oxide (Gd<sub>2</sub>O<sub>3</sub>) contents (0, 5, 10, 15, and 20 wt%). The results indicate that the overall thermal-neutron-shielding properties of the r-HDPE composites were enhanced with the addition of Gd<sub>2</sub>O<sub>3</sub>, as evidenced by large reductions in I/I<sub>0</sub>, HVL, and TVL, as well as the substantial increases in  $\Sigma_t$  and  $\Sigma_{t/\rho}$  of the composites. Furthermore, the results reveal that the values for tensile properties initially increased up to 5–15 wt% of Gd<sub>2</sub>O<sub>3</sub> and then gradually decreased at higher contents. In addition, the results show that the addition of Gd<sub>2</sub>O<sub>3</sub> particles generally increased the density ( $\rho$ ), the remaining ash at 600 °C, and the degree of crystallinity (%XC) of the composites. This work also determined the effects of gamma irradiation on relevant properties of the composites. The findings indicate that following gamma aging, the tensile modulus slightly increased, while the tensile strength, elongation at break, and hardness (Shore D) showed no significant ( $p < 0.05$ ) differences, except for the sample containing 5 wt% of Gd<sub>2</sub>O<sub>3</sub>, which exhibited a noticeable reduction in elongation at break. Furthermore, by comparing the neutron-shielding and mechanical properties of the developed r-HDPE composites with common borated polyethylene (PE) containing 5 wt% and 15 wt% of boron, the results clearly indicate the superior shielding and tensile properties in the r-HDPE composites, implying the great potential of r-HDPE composites to replace virgin plastics as effective and more eco-friendly shielding materials.

**Keywords:** recycled materials; neutrons; attenuation; rare-earth oxide; mechanical properties; gamma aging



**Citation:** Toyen, D.; Wimolmala, E.; Hemvichian, K.; Lertsarawut, P.; Saenboonruang, K. Highly Efficient and Eco-Friendly Thermal-Neutron-Shielding Materials Based on Recycled High-Density Polyethylene and Gadolinium Oxide Composites. *Polymers* **2024**, *16*, 1139. <https://doi.org/10.3390/polym16081139>

Academic Editor: Florian Part

Received: 6 March 2024

Revised: 11 April 2024

Accepted: 16 April 2024

Published: 18 April 2024



**Copyright:** © 2024 by the authors. Licensee MDPI, Basel, Switzerland. This article is an open access article distributed under the terms and conditions of the Creative Commons Attribution (CC BY) license (<https://creativecommons.org/licenses/by/4.0/>).

## 1. Introduction

Radiation technologies, particularly those involving neutrons, have seen major advancements and widespread application across various fields. These applications include

neutron imaging in materials science and medicine [1,2], Boron Neutron Capture Therapy (BNCT) for treating brain cancers [3], the production of radioisotopes for medical diagnostics [4], power generation through nuclear fission and nuclear fusion [5,6], and moisture measurements in field applications [7]. These technologies not only enhance product quality, but often also present more environmentally friendly alternatives to conventional methods [8]. Nevertheless, it is crucial to acknowledge that excessive exposure to ionizing radiation can pose severe risks, especially to humans, potentially leading to organ abnormalities and even loss of life [9,10]. Consequently, strict safety protocols must be followed by all nuclear and radiation-related facilities to ensure the well-being of personnel, users, and the surrounding public [11].

Within the framework of the “ALARA” principle (As Low As Reasonably Achievable), one of the three fundamental approaches for bolstering the safety of relevant users involves the utilization of efficient and appropriate shielding equipment. The choice of materials and designs for such equipment depends on various factors, including the type and energy of the radiation, space constraints, and the intended application [12,13]. Particularly for neutron shielding equipment, commonly used materials include natural and synthetic rubbers (NR and SR, respectively), polyethylene (PE), paraffin, and epoxy [14–16]. These materials are suitable for such purposes due to their high contents of lightweight elements, particularly hydrogen (H) and carbon (C), within their chemical compositions. These elements efficiently scatter incoming neutrons, leading to substantial energy losses and necessitating fewer scatters to sufficiently lower neutron intensities compared to those containing heavier elements [17].

Although the previously mentioned polymers can effectively reduce neutron intensity through elastic scattering, their efficiency in shielding, particularly against thermal neutrons, can be substantially enhanced by incorporating them with compounds having a high neutron absorption cross section ( $\sigma_{\text{abs}}$ ), such as boron carbide ( $\text{B}_4\text{C}$ ), boron oxide ( $\text{B}_2\text{O}_3$ ), boron nitride (BN), and boric acid ( $\text{H}_3\text{BO}_3$ ) [18–21]. The addition of boron compounds introduces a more efficient and superior mechanism for attenuating thermal neutrons through neutron absorption, resulting in less materials being needed to achieve adequate safety and protection. Some examples of the utilization of boron compounds in neutron shielding include the addition of BN into ultrahigh molecular weight polyethylene fiber (UPEF) and polyurethane (PU) composites, where the results indicated a substantial increase in the linear attenuation coefficient ( $\mu$ ) values, rising from  $6 \text{ cm}^{-1}$  in UPEF/PU composites to  $22 \text{ cm}^{-1}$  in 20 wt% BN/UPEF/PU composites, producing a roughly 3.5-fold improvement [22]. Another example involves the addition of  $\text{B}_2\text{O}_3$  into wood/NR composites, which resulted in enhanced attenuating capabilities of the materials, as shown by a reduction in neutron transmission ratios ( $I/I_0$ ) from 95.6% in a 2.5 mm thick wood/NR sample to 60.2% in a 2.5 mm thick sample containing 80 parts per hundred parts of rubber by weight (phr), producing a roughly nine-fold improvement [23,24].

Apart from boron compounds, there has been major interest among researchers in utilizing rare-earth oxides, particularly gadolinium oxide ( $\text{Gd}_2\text{O}_3$ ), as potential substitutes for traditional boron compounds. This is due to gadolinium (Gd) offering a substantially higher  $\sigma_{\text{abs}}$  than that of boron (B), with the  $\sigma_{\text{abs}}$  values for Gd and B being 49,700 and 767 barns, respectively [25], making  $\text{Gd}_2\text{O}_3$  a superior thermal neutron absorber than boron compounds at the same content [26]. In addition to its effectiveness as a neutron absorber, Gd also has a relatively high atomic number ( $Z$ ) of 64, as well as a high density ( $\rho$ ) of  $\text{Gd}_2\text{O}_3$  ( $\rho = 7.41 \text{ g/cm}^3$ ), making the compound well suited for attenuating gamma rays through photoelectric absorption, Compton scattering, and pair production [26,27]. Consequently, materials containing  $\text{Gd}_2\text{O}_3$  can simultaneously attenuate both thermal neutrons and secondary gamma rays that are often produced following neutron absorption, distinguishing them from boron-based composites by eliminating the need for additional layers of lead (Pb) or other heavy-metal materials as gamma shielding [28,29].

In addition to the choice of fillers, main materials also play pivotal roles in defining the properties and practical utility of the products. While there is a range of materials

available for manufacturing neutron-shielding products, HDPE ((C<sub>2</sub>H<sub>4</sub>)<sub>n</sub>) stands out as a prevalent and efficient polymer for applications that require strength and rigidity, such as construction parts, partitions, and containers for radioactive sources, due to its exceptional strength, durability, and cost-effectiveness [30], as well as its high carbon (C) and hydrogen (H) contents, which are suitable for neutron scattering [31]. Nevertheless, the growing demands for HDPE, both in households and industries, have raised serious concerns regarding the plastic pollution in oceans and landfills that severely harm humans, animals, plants, and the environment in general [32]. As a result, this drawback from the increasing utilization of HDPE has hindered its usefulness and underscored the need to reduce the accumulation of HDPE in the environment through recycling process so that the recycled products/tools can be sufficiently and safely used again [33,34]. Specifically for recycled HDPE (r-HDPE) in radiation protection, there have been several works aimed at creating effective shielding products that yielded promising outcomes and impacts. For example, r-HDPE was incorporated with lead oxide (PbO) nanoparticles for gamma protection, with the results demonstrating that the composites could effectively attenuate gamma rays at energies of 59.53, 661.66, 1173.25, and 1332.50 keV, as evidenced by the high values of the linear attenuation coefficient ( $\mu$ ) of 5.760, 0.241, 0.146, and 0.134 cm<sup>-1</sup>, respectively, as determined at 50 wt% PbO [35]. This example not only underscores the great potential of utilizing r-HDPE in radiation protection, but also offers a sustainable alternative to virgin plastics that would conserve valuable natural resources, as well as reduce energy consumption and greenhouse gas emissions during production [36].

To further advance the progress in the development of radiation-shielding products using recycled materials and to expand their potential applications to neutron shielding, the present research determined the optimum formulation and process for the preparation of Gd<sub>2</sub>O<sub>3</sub> particles through a surface treatment using a silane coupling agent (3-aminopropyltriethoxysilane; KBE903), by considering the effects of KBE903 on the mechanical and neutron-shielding properties of the composites [37]. Furthermore, with the optimal silane content determined, varying contents of treated Gd<sub>2</sub>O<sub>3</sub>, (0, 5, 10, 15, and 20 wt%) were incorporated into r-HDPE, and important properties of interest were comprehensively examined and compared in terms of the following: thermal neutron shielding (the total macroscopic cross section ( $\Sigma_t$ ), the mass attenuation coefficient ( $\Sigma_{t,\rho}$ ), the half-value layer (HVL), and the tenth value layer (TVL)), mechanical (tensile modulus, tensile strength, elongation at break, and hardness (Shore D)), morphological (SEM images), physical (density), and thermal (thermogravimetric analysis) properties. Additionally, since degradation due to exposure to radiation during actual use was possible, changes in the mechanical and thermal-neutron-shielding properties of the composites under 70 kGy gamma aging were determined and compared with those of non-aged samples. The outcomes of this research should not only provide in-depth insights into the advancement of enhanced thermal-neutron-shielding materials using r-HDPE composites with the addition of rare-earth oxides, but also elucidate the optimal processes for sample preparation involving surface treatment, which could potentially maintain or even enhance specific properties of the composites.

## 2. Materials and Methods

### 2.1. Surface Treatment of Gd<sub>2</sub>O<sub>3</sub> Particles

The Gd<sub>2</sub>O<sub>3</sub> particles were acquired from the Richest Group (Shanghai, China). Figure 1a,b show optical and micrograph images, respectively, of Gd<sub>2</sub>O<sub>3</sub>, illustrating the colors, shapes, and sizes of the particles used in this work. The distribution of particle sizes, determined using a laser diffraction technique (Mastersizer-2000; Malvern Instruments Limited; Malvern, UK), with a particle size analysis range of 0.02–15  $\mu$ m, is shown in Figure 1c, revealing an average particle size of 3.08  $\mu$ m.

Due to the poor interfacial compatibility between the HDPE and Gd<sub>2</sub>O<sub>3</sub> surfaces [38], the Gd<sub>2</sub>O<sub>3</sub> particles were surface-treated using a silane coupling agent (3-aminopropyltriethoxysilane; KBE903) prior to compounding with the r-HDPE samples. To initiate the treatment proce-

dure, KBE903, ethanol, and distilled water, with their respective contents shown in Table 1, were thoroughly mixed for 15 min using a magnetic stirrer (RSM-01; Phoenix; Mannheim, Germany). Subsequently, the  $Gd_2O_3$  particles were introduced into the mixture and stirred for an additional 30 min at a rotational speed of 1000 rpm. Then, the mixture was transferred to a water bath, and the stirring continued for 1 h at a water temperature of 90 °C. After stirring, the mixture was oven dried (ED/FD; Binder; Tuttlingen, Germany) at 80 °C for 3 h to eliminate any residual ethanol and distilled water, before being stored in sealed containers for subsequent processing and characterization.

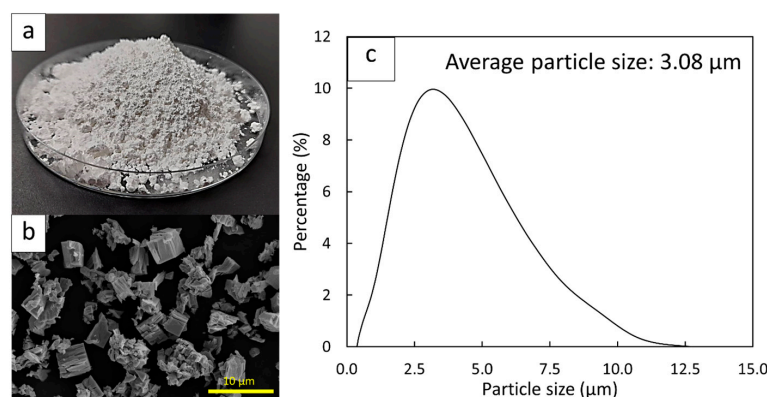


**Figure 1.** (a) Optical and (b) micrograph images of  $Gd_2O_3$  particles and (c) distribution of  $Gd_2O_3$  particle sizes.

**Table 1.** Formulations, with names, contents, and suppliers for surface treatment of  $Gd_2O_3$  particles.

Chemical	Content (g)	Supplier
$Gd_2O_3$	100	Richest Group (Shanghai, China)
Silane coupling agent (KBE903)	A *	Kisco(T) Ltd. (Bangkok, Thailand)
99% Ethanol	92 – A	Gammaco Co., Ltd. (Nonthaburi, Thailand)
Distilled water	8	Kasetsart University (Bangkok, Thailand)

\* A = 0, 5, 10, 15, or 20.

## 2.2. Preparation of $Gd_2O_3$ /r-HDPE Samples

r-HDPE granules, with a melt flow index of 0.55 g/10 min, was kindly provided by S.P. Plastic Industry (Bangkok, Thailand). To prepare the samples, r-HDPE and treated  $Gd_2O_3$ , with contents as shown in Table 2, were continuously mixed using a high-speed mixer (LMXZ; Lab Tech Engineer; Samut Prakan, Thailand) and then compounded using a twin-screw extruder (CTW 1000C; Haake Rheomax; Leipzig, Germany), with the temperatures for feed, plastification, mixing, and die zones being 175, 180, 185, and 190 °C, respectively, at a screw speed of 60 rpm. The  $Gd_2O_3$ /r-HDPE samples with dimensions of 18 cm × 9 cm and a thickness of 2 mm were formed by molding the granules using a hot press (LP-20M LMXS; Lab Tech Engineering; Samut Prakan, Thailand) at a pressure of 15 MPa and a temperature of 190 °C for 8 min. Notably, the content of  $Gd_2O_3$  was kept at 20 wt% (the maximum content of  $Gd_2O_3$  investigated in this work) during the silane optimization procedure (Part I). Following the completion of Part I, the optimum KBE903 content was obtained and subsequently used for the preparation of samples with varying  $Gd_2O_3$  contents from 0 to 20 wt% (Part II). Figure 2a,b illustrate the overall scope of this work, including Parts I and II, respectively.

**Table 2.** Formulations, with names, contents, and suppliers for preparation of  $Gd_2O_3$ /r-HDPE samples.

Chemical	Content (wt%)	Supplier
$Gd_2O_3$	B *	Richest Group (Shanghai, China)
r-HDPE	100 – B	S.P. Plastic Industry (Bangkok, Thailand)

\* B = 0, 5, 10, 15, or 20.

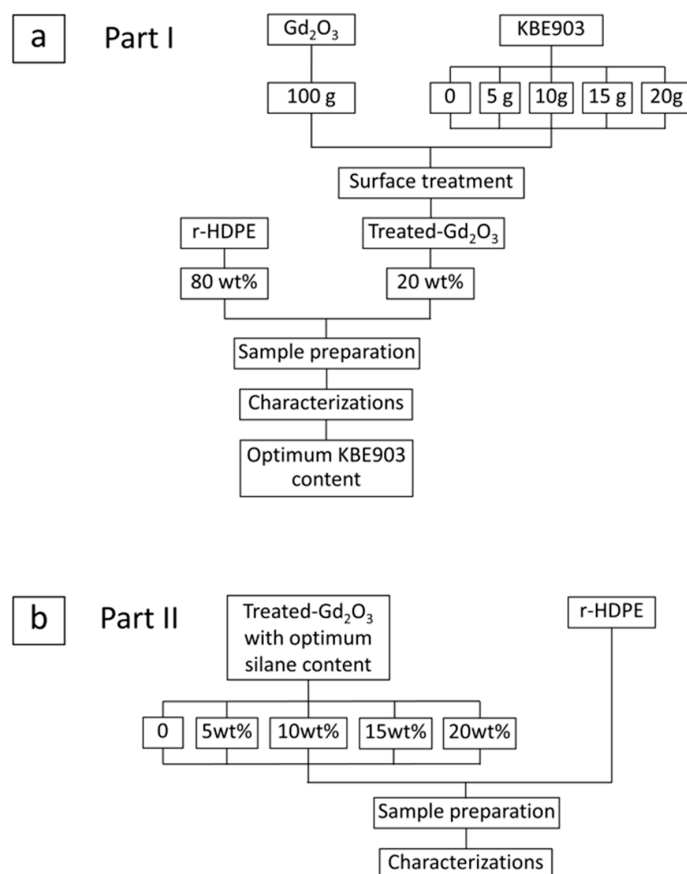


**Figure 2.** Scope of work showing (a) Part I, optimization procedure for surface treatment of  $Gd_2O_3$  particles using silane coupling agent (KBE903), and (b) Part II, preparation and investigation of properties for  $Gd_2O_3$ /r-HDPE composites with varying  $Gd_2O_3$  contents.

### 2.3. Gamma Irradiation on $Gd_2O_3$ /r-HDPE Samples

To understand the effects of gamma irradiation (gamma aging) on the properties of  $Gd_2O_3$ /r-HDPE composites, all samples were gamma irradiated with a total dose of 70 kGy using a gamma irradiator equipped with a  $^{60}Co$  source (Ob-servo ignis-09; Institute of Isotopes Co., Ltd.; Budapest, Hungary) with a dose rate of 9.2 kGy/h at the Thailand Institute of Nuclear Technology (Public Organization). Then, the changes in the thermal-neutron-shielding and mechanical properties for all samples under gamma aging were compared with those of non-aged samples.

### 2.4. Characterization

#### 2.4.1. Thermal-Neutron-Shielding Properties

A narrow-beam neutron source ( $^{47}Ci$   $^{241}Am/Be$ ) enclosed in a paraffin container was used. A stack of 5 cm thick HDPE sheets positioned in front of the r-HDPE samples served as a moderator to thermalize the 4.5-MeV neutrons from the source. Then, the transmitted neutrons were detected using a cylindrical  $^3He$  neutron detector (Model 251; LND; Ocean-side, NY, USA) with a diameter of 12.7 mm. The detector was connected to a high-voltage power supply (Model 659; Ortec; Atlanta, GA, USA), a preamplifier/amplifier (Model 2022; Canberra; Atlanta, GA, USA), and a counter (Model 535P; Tennelec; Oak Ridge, TN, USA). For each formulation, 5 independent tests, each lasting 60 s, were conducted, and the average counts (I) of the transmitted neutrons were recorded. Additionally, the initial count ( $I_0$ ) was recorded, representing the neutron count in the absence of any samples. The determination of thermal-neutron-shielding parameters consisted of neutron transmission ratios ( $I/I_0$ ), the total macroscopic cross section ( $\Sigma_t$ ), the mass attenuation coefficient ( $\Sigma_{t/\rho}$ ), the half-value layer (HVL), and the tenth value layer (TVL). The corresponding equations for the calculations of

these parameters as well as the graphical setup of the neutron shielding tests are available elsewhere [17].

#### 2.4.2. Density and Degree of Crystallinity

The densities for all Gd<sub>2</sub>O<sub>3</sub>/r-HDPE composites were measured using a densitometer (MH-300A; Shanghai, China) with a precision of 0.01 g/cm<sup>3</sup>, following Archimedes' principle [39] and ASTM D792-13 standard testing [40]. In addition, the theoretical densities ( $\rho_t$ ) of the Gd<sub>2</sub>O<sub>3</sub>/r-HDPE composites were determined to identify any discrepancies between the calculated and actual densities. The theoretical densities were calculated using Equations (1) and (2) [27]:

$$\rho_t = \frac{100}{\left(\frac{C_{r\text{-HDPE}}}{\rho_{r\text{-HDPE}}}\right) + \left(\frac{C_{\text{Gd}_2\text{O}_3}}{\rho_{\text{Gd}_2\text{O}_3}}\right)} \quad (1)$$

where  $C_{r\text{-HDPE}}$ ,  $C_{\text{Gd}_2\text{O}_3}$ ,  $\rho_{r\text{-HDPE}}$ , and  $\rho_{\text{Gd}_2\text{O}_3}$  are the r-HDPE content (wt%), the Gd<sub>2</sub>O<sub>3</sub> content (wt%), the density of r-HDPE (0.93 g/cm<sup>3</sup>), and the density of Gd<sub>2</sub>O<sub>3</sub> (7.41 g/cm<sup>3</sup>), respectively.

In addition, the degree of crystallinity (%XC) of the composites, which represents the percentage of crystalline regions in the sample, was assessed using X-ray diffraction (XRD; D8 Advance; Bruker; Mannheim, Germany) with Ni-filtered CuK $\alpha$  radiation within a scanning angle range of 10°–80° (2 $\theta$ ) and a scanning speed of 0.02°/step. The %XC was determined by finding the ratio of the area under the crystalline peak ( $A_C$ ) to the sum of the area of all crystalline and amorphous peaks ( $A_T$ ) as shown in Equation (2) [41,42]:

$$\%XD = \frac{A_C}{A_T} \times 100\% \quad (2)$$

#### 2.4.3. Morphology and Elemental Composition Analysis

The determination of morphology, the dispersion of Gd<sub>2</sub>O<sub>3</sub> particles, the distribution of Gd elements in the r-HDPE matrix, and the elemental composition of the Gd<sub>2</sub>O<sub>3</sub>/r-HDPE composites was conducted using scanning electron microscopy (SEM) (Quanta 450; FEI; Brno-Černovice, Czech Republic) and energy-dispersive X-ray (EDX) spectroscopy (X-Max; Oxford Instruments; Abingdon, UK). For the determination of the morphologies of the fractured surfaces, all samples were immersed in liquid nitrogen for 5 min and then abruptly snapped. Notably, all specimens were coated with a 0.2 mm thick layer of gold using a magnetron sputter (SC7620; Quorum Technologies Polaron; Hertfordshire, UK) at a current of 5 mA for 120 s prior to the SEM-EDX investigations in order to improve electrical conductivity on the sample surface to avoid effects of charge accumulation that may distort or reduce image quality.

#### 2.4.4. Functional Groups and Thermal Properties

The identification of active functional groups presented on both the untreated and treated Gd<sub>2</sub>O<sub>3</sub> particles was carried out using Fourier-transform infrared (FTIR) spectroscopy; (Vertex 70; Bruker; Billerica, MA, USA), covering wavenumbers within the range 400–4000 cm<sup>-1</sup>. The thermal properties of all the Gd<sub>2</sub>O<sub>3</sub>/r-HDPE composites were determined through thermogravimetric analysis (TGA; TGA/DSC2/LF/1100; Mettler Toledo; Greifensee, Switzerland), with 0.4 mg of each sample enclosed in an aluminum oxide crucible and subjected to heating from room temperature to 800 °C, at a scanning rate of 20 °C/min (under a nitrogen atmosphere).

#### 2.4.5. Mechanical Properties

The mechanical properties, consisting of the tensile modulus, tensile strength, and elongation at break, for all the Gd<sub>2</sub>O<sub>3</sub>/r-HDPE composites were assessed using a Universal Testing Machine (TM-G5K; TM Tech Testing Co., Ltd.; Bangkok, Thailand). The testing procedure adhered to the ASTM D638-14 standard [43] testing at a testing speed of 50 mm/min. For the surface hardness measurements, the samples were tested using a durometer (GS-719G;

Teclock; Nagano, Japan) according to ASTM D2240–03 [44] (Shore D) standard testing. Notably, a minimum of 3 repetitions for each formulation was carried out for all mechanical measurements.

### 2.5. Statistical Analysis

A level of 95% significance ( $p < 0.05$ ) was used for the descriptive analysis of the data. A Student's *t*-test was also applied to determine any significant differences between the results of interest. The statistical analyses were conducted using the IBM SPSS Statistics 20 software (New York, NY, USA) [17].

## 3. Results and Discussion

### 3.1. Optimization for Surface Treatment of $Gd_2O_3$ Particles

#### 3.1.1. Functional Groups

The functional groups of KBE903, non-treated  $Gd_2O_3$ , and treated  $Gd_2O_3$  particles, determined using FTIR, are shown in Figure 3. For the spectra of KBE903 (Figure 3a), dominant peaks were observed at  $475\text{ cm}^{-1}$  (Si–O–Si),  $700\text{ cm}^{-1}$  (C–H),  $770\text{ cm}^{-1}$  (Si–O–C),  $865\text{ cm}^{-1}$  (Si–O),  $950\text{ cm}^{-1}$  (Si–O),  $1066\text{ cm}^{-1}$  (Si–O),  $1167\text{ cm}^{-1}$  (Si–O–C),  $1300\text{ cm}^{-1}$  (C–O),  $1390\text{ cm}^{-1}$  (O–H),  $1450\text{ cm}^{-1}$  (C–H),  $1600\text{ cm}^{-1}$  (N–H), and  $2880\text{--}2980\text{ cm}^{-1}$  (C–H) [45,46], while dominant peaks for the non-treated  $Gd_2O_3$  were observed at  $445\text{ cm}^{-1}$  and  $545\text{ cm}^{-1}$ , corresponding to the stretching vibration of  $Gd_2O_3$ , and  $1020\text{--}1060\text{ cm}^{-1}$ , corresponding to the stretching vibrations of Gd–O bonds [37]. For the treated  $Gd_2O_3$  particles, the FTIR spectra (Figure 3b) showed an additional broad peak at  $1116\text{ cm}^{-1}$  (Si–O–C) (in addition to peaks at  $445\text{ cm}^{-1}$ ,  $545\text{ cm}^{-1}$ , and  $1020\text{--}1060\text{ cm}^{-1}$ ) with their amplitudes increasing with the KBE903 contents. These additional peaks, as well as the observed correlation between peak amplitudes and KBE903 contents, clearly imply the successful treatment of  $Gd_2O_3$  particles by grafting KBE903 on the surfaces of  $Gd_2O_3$  [47]. It should be noted that there was a shift in the Si–O–C spectrum from  $1167\text{ cm}^{-1}$  in KBE903 to  $1116\text{ cm}^{-1}$  in the treated  $Gd_2O_3$  particles, which could possibly be due to the effects of hydrolysis during the treatment process that changed the degree of hydrolysis and condensation of KBE903, influencing the Si–O–C peak positions in the composites [48]. Another plausible explanation of the shift in the FTIR spectra could be due to the merger between the  $1066\text{ cm}^{-1}$  (Si–C) and  $1167\text{ cm}^{-1}$  (Si–O–C) peaks of KBE903, resulting in a new broader peak at  $1116\text{ cm}^{-1}$ .

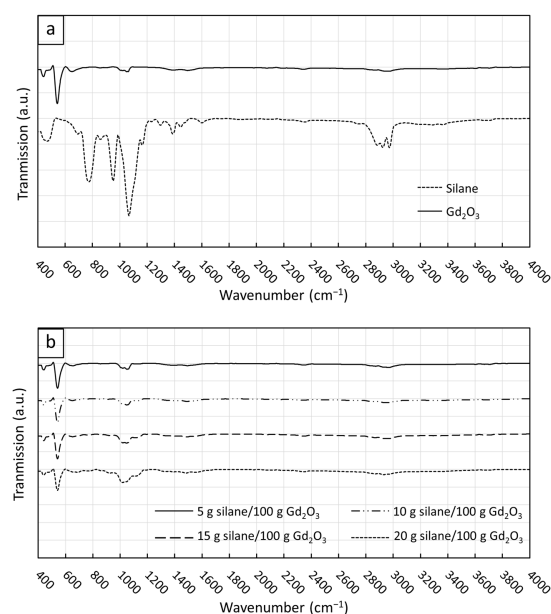


**Figure 3.** Functional groups determined using FTIR of (a) silane coupling agent (KBE903) and non-treated  $Gd_2O_3$  particles and (b) treated  $Gd_2O_3$  particles with varying KBE903 contents (5, 10, 15, and 20 g/100 g  $Gd_2O_3$ ).

### 3.1.2. Density and Elemental Composition

The densities of the 20 wt% Gd<sub>2</sub>O<sub>3</sub>/r-HDPE composites are shown in Table 3; there were no significant differences among the densities for all samples, with the values being in the range 1.11–1.13 g/cm<sup>3</sup>. These measured densities were in good agreement with the theoretical value of 1.13 g/cm<sup>3</sup>, derived using Equation (1), with slight differences possibly due to the presence of voids in the r-HDPE matrix that reduced the final mass of the samples.

**Table 3.** Densities and elemental compositions of 20 wt% Gd<sub>2</sub>O<sub>3</sub>/r-HDPE composites, with varying silane (KBE903) contents (0, 5, 10, 15, and 20 g/100 g Gd<sub>2</sub>O<sub>3</sub>). The values are shown as the mean ± standard deviation of the mean.

Silane Content (g/100 g Gd <sub>2</sub> O <sub>3</sub> )	Density (g/cm <sup>3</sup> )	Elemental Composition (% by Weight)			
		C	O	Si	Gd
0	1.11 ± 0.01	73.47 ± 4.32	6.11 ± 1.37	0.02 ± 0.01 *	20.41 ± 1.56
5	1.11 ± 0.02	74.37 ± 2.02	4.66 ± 1.29	0.06 ± 0.02	20.91 ± 0.73
10	1.13 ± 0.01	74.19 ± 2.74	4.30 ± 0.95	0.11 ± 0.06	21.40 ± 1.90
15	1.13 ± 0.02	73.47 ± 1.18	3.98 ± 1.13	0.23 ± 0.13	22.33 ± 1.88
20	1.12 ± 0.01	74.51 ± 2.60	5.25 ± 0.27	0.26 ± 0.05	19.98 ± 2.79

\* The small content of Si in non-treated Gd<sub>2</sub>O<sub>3</sub> could be due to a small contamination of silane in the equipment used during the treatment process. However, the Si content was small in that it had negligible effects for the determination of optimum silane content.

Table 3 also shows the elemental composition of the 20 wt% Gd<sub>2</sub>O<sub>3</sub>/r-HDPE composites, with varying KBE903 contents (0–20 g/100 g Gd<sub>2</sub>O<sub>3</sub>). The results indicate that the compositions of Gd for all samples were not significantly different, with the values being in the range 19.98–22.33% (by weight). On the other hand, the compositions of Si increased with increasing KBE903 contents, implying the presence of KBE903 in the composites and a successful surface treatment of Gd<sub>2</sub>O<sub>3</sub> particles.

### 3.1.3. Thermal-Neutron-Shielding Properties

The thermal-neutron-shielding properties, consisting of  $I/I_0$ ,  $\Sigma_t$ ,  $\Sigma_{t/\rho}$ , and HVL, for all 20 wt% Gd<sub>2</sub>O<sub>3</sub>/r-HDPE samples are shown in Table 4, which indicate that the sample containing Gd<sub>2</sub>O<sub>3</sub> treated with 5 g of KBE903 per 100 g of Gd<sub>2</sub>O<sub>3</sub> had the highest thermal-neutron-shielding properties compared to those treated with other KBE903 contents, as evidenced by the lowest values for  $I/I_0$  and HVL, and the highest values of  $\Sigma_t$  and  $\Sigma_{t/\rho}$  in the former. These differences in the shielding abilities for each condition could be explained by the distribution of Gd elements in the composites, as illustrated in Gd mapping images (Figure 4), which clearly reveal substantially more uniform dispersion and distribution of Gd elements in the sample with 5 g of KBE903 (Figure 4a). Consequently, incoming thermal neutrons could better interact and be absorbed by the Gd elements in the former, subsequently leading to higher overall shielding properties for the materials [37]. Notably, more particle agglomerations were observed in Figure 4b–d due to the excessive use of KBE903 that led to the initiation of self-agglomeration or the poor distribution of Gd<sub>2</sub>O<sub>3</sub> particles, contributing to the increases in the values of  $I/I_0$  for the samples with 10–20 g of KBE903 per 100 g of Gd<sub>2</sub>O<sub>3</sub> [49]. The self-agglomeration observed in the case of samples with excessive silane could have been because the surface of Gd<sub>2</sub>O<sub>3</sub> becoming saturated with silane molecules, leading to a multilayer formation of silane that acted as a bridge between Gd<sub>2</sub>O<sub>3</sub> particles, subsequently facilitating the agglomerations of the particles [50].

**Table 4.** Thermal-neutron-shielding properties, consisting of neutron transmission ratio ( $I/I_0$ ), total macroscopic cross section ( $\Sigma_t$ ), mass attenuation coefficient ( $\Sigma_{t/\rho}$ ), and half-value layer (HVL), of 20 wt%  $Gd_2O_3$ /r-HDPE composites, with varying silane (KBE903) contents (0, 5, 10, 15, and 20 g/100 g  $Gd_2O_3$ ). The values are shown as the mean  $\pm$  standard deviation of the mean.

Silane Content (g/100 g $Gd_2O_3$ )	$I/I_0$ *	$\Sigma_t$ ( $cm^{-1}$ )	$\Sigma_{t/\rho}$ ( $cm^2/g$ )	HVL (cm)
0	$0.72 \pm 0.01$	$1.89 \pm 0.08$	$1.70 \pm 0.08$	$0.37 \pm 0.02$
5	$0.47 \pm 0.01$	$4.23 \pm 0.03$	$3.80 \pm 0.03$	$0.16 \pm 0.01$
10	$0.65 \pm 0.02$	$2.35 \pm 0.20$	$2.08 \pm 0.18$	$0.30 \pm 0.03$
15	$0.65 \pm 0.01$	$2.35 \pm 0.07$	$2.08 \pm 0.06$	$0.30 \pm 0.01$
20	$0.56 \pm 0.01$	$3.35 \pm 0.14$	$3.02 \pm 0.12$	$0.21 \pm 0.01$

\* Values of  $I/I_0$  were determined using 2 mm thick samples.

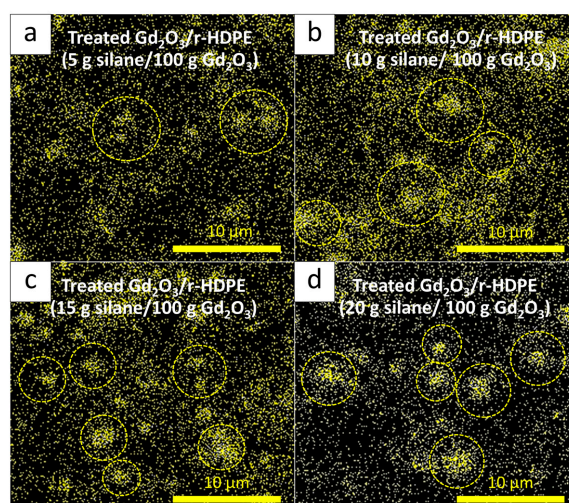


**Figure 4.** SEM-EDX mapping showing the distribution of Gd elements in the 20 wt%  $Gd_2O_3$ /r-HDPE composites, with varying silane (KBE903) contents of (a) 5 g, (b) 10 g, (c) 15 g, and (d) 20 g per 100 g of  $Gd_2O_3$ . Dotted circles indicate areas with Gd agglomeration.

#### 3.1.4. Mechanical Properties

Table 5 presents the mechanical properties, consisting of the tensile modulus, tensile strength, elongation at break, and hardness (shore D), for the 20 wt%  $Gd_2O_3$ /r-HDPE composites, with the results showing a pattern similar to the thermal-neutron-shielding properties discussed in Section 3.1.3. Specifically, it was observed that the composites containing  $Gd_2O_3$  treated with KBE903 with a content of 5 g/100 g  $Gd_2O_3$  had the highest overall mechanical properties, as evidenced by their superior tensile modulus, tensile strength, and elongation at break compared to those under other conditions. This improvement in the mechanical properties of the former could have been due to the improved interfacial compatibility between the r-HDPE matrix and the treated- $Gd_2O_3$  particles, which resulted in the enhanced abilities of the materials to transfer and withstand external forces [51]. Figure 5, which shows the morphologies of the fractured surfaces of the samples, reveals visible voids, as well as clear  $Gd_2O_3$  particles at the fractures, especially those without KBE903 treatment (Figure 5a) or with excessive KBE903 contents (Figure 5c). These observations indicate that the fractures occurred at voids or interfaces between the r-HDPE matrix and  $Gd_2O_3$  particles, implying poor interfacial compatibility between the two substances [52]. On the other hand, Figure 5b shows that the  $Gd_2O_3$  particles that were treated with 5 g of KBE903 per 100 g of  $Gd_2O_3$ , were mostly embedded/covered in the r-HDPE matrix at the fractured surface, implying better interfacial compatibility and hence higher overall values for the mechanical properties of the composites [53]. Notably, the hardness (Shore D) values of all samples were not significantly different, with the values being in the range 53–55.

**Table 5.** Mechanical properties, consisting of tensile modulus, tensile strength, elongation at break, and hardness (Shore D), of 20 wt% Gd<sub>2</sub>O<sub>3</sub>/r-HDPE composites, with varying silane (KBE903) contents (0, 5, 10, 15, and 20 g/100 g Gd<sub>2</sub>O<sub>3</sub>). The values are shown as the mean ± standard deviation of the mean.

Silane Content (g/100 g Gd <sub>2</sub> O <sub>3</sub> )	Tensile Modulus (MPa)	Tensile Strength (MPa)	Elongation at Break (%)	Hardness (Shore D)
0	154.6 ± 4.3	17.7 ± 0.3	35.0 ± 2.4	54 ± 3
5	173.4 ± 14.5	19.6 ± 0.4	51.6 ± 2.3	53 ± 4
10	65.6 ± 10.0	15.6 ± 2.4	20.9 ± 3.6	53 ± 3
15	100.5 ± 27.8	16.0 ± 1.5	26.3 ± 3.3	55 ± 2
20	69.7 ± 8.9	17.3 ± 1.5	24.7 ± 4.6	53 ± 3

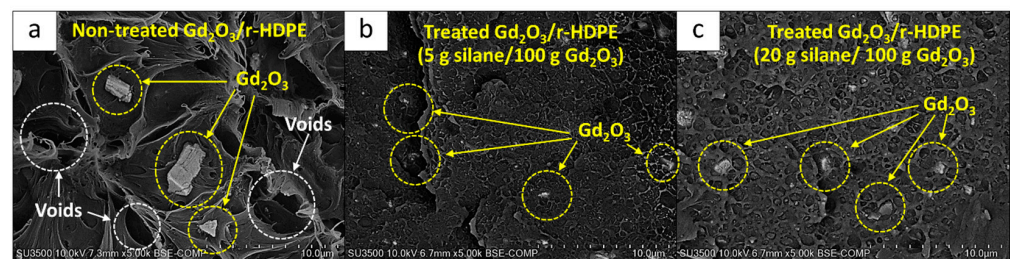


**Figure 5.** SEM images showing fractured surfaces of 20 wt% Gd<sub>2</sub>O<sub>3</sub>/r-HDPE composites with varying KBE903 contents of (a) 0, (b) 5 g, and (c) 20 g per 100 g of Gd<sub>2</sub>O<sub>3</sub>.

As discussed in Sections 3.1.3 and 3.1.4, it was evident that using a KBE903 content of 5 g/100 g Gd<sub>2</sub>O<sub>3</sub> for the surface treatment of Gd<sub>2</sub>O<sub>3</sub> resulted in the highest overall thermal-neutron-shielding and mechanical properties for the Gd<sub>2</sub>O<sub>3</sub>/r-HDPE composites (Tables 4 and 5). Consequently, this particular KBE903 content, along with the developed surface treatment procedure, was chosen as the optimum condition for preparing Gd<sub>2</sub>O<sub>3</sub> particles that were subsequently used for the preparation of Gd<sub>2</sub>O<sub>3</sub>/r-HDPE samples (with varying Gd<sub>2</sub>O<sub>3</sub> contents) in Part II.

### 3.2. Effects of Gd<sub>2</sub>O<sub>3</sub> Contents on Properties of Gd<sub>2</sub>O<sub>3</sub>/r-HDPE Composites

#### 3.2.1. Density and Elemental Composition of Gd<sub>2</sub>O<sub>3</sub>/r-HDPE Composites

The theoretical and measured densities of all Gd<sub>2</sub>O<sub>3</sub>/r-HDPE composites, with varying Gd<sub>2</sub>O<sub>3</sub> contents (0, 5, 10, 15, and 20 wt%), are shown in Table 6. The results indicate that the densities of the samples increased with increasing Gd<sub>2</sub>O<sub>3</sub> contents. This could have been due to the higher density of Gd<sub>2</sub>O<sub>3</sub> than that of the r-HDPE, which resulted in an increased mass of the sample per unit volume after the addition of Gd<sub>2</sub>O<sub>3</sub> ( $\rho_{\text{r-HDPE}} = 0.93 \text{ g/cm}^3$  and  $\rho_{\text{Gd}_2\text{O}_3} = 7.41 \text{ g/cm}^3$ ). Furthermore, it was found that the measured densities agreed with the theoretical ones, implying that the samples were well prepared. In addition, Table 6 shows the elemental compositions of the Gd<sub>2</sub>O<sub>3</sub>/r-HDPE composites, indicating that the composites were mainly composed of C, O, Si, and Gd (H was not detectable due to the detection limitation of SEM-EDX) [54]. Notably, the compositions of Gd were largely related to the nominal Gd<sub>2</sub>O<sub>3</sub> contents, which partly confirmed that the samples were correctly prepared.

**Table 6.** Densities and elemental compositions of Gd<sub>2</sub>O<sub>3</sub>/r-HDPE composites, with varying Gd<sub>2</sub>O<sub>3</sub> contents (0, 5, 10, 15, and 20 wt%). The values are shown as the mean ± standard deviation of the mean.

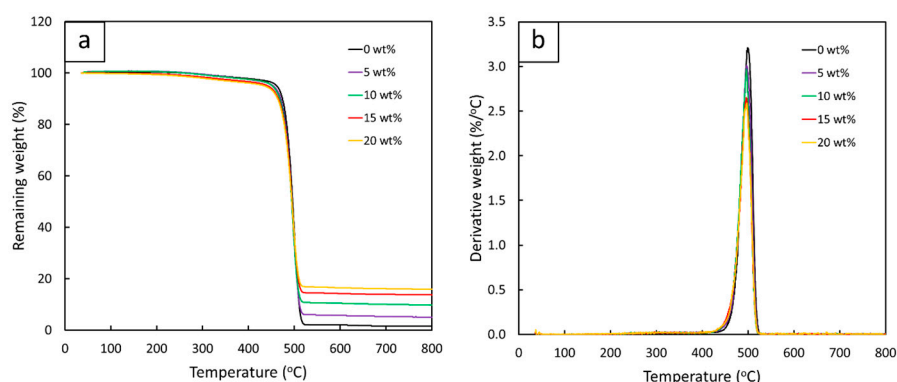
Gd <sub>2</sub> O <sub>3</sub> Content (wt%)	Density (g/cm <sup>3</sup> )		Elemental Composition (% by Weight)			
	Measured	Theoretical	C	O	Si	Gd
0	0.93 ± 0.01	0.93	96.35 ± 1.08	3.65 ± 1.08	n/a	n/a
5	0.97 ± 0.02	0.97	89.60 ± 1.51	3.44 ± 0.43	0.07 ± 0.02	6.89 ± 1.25

Table 6. Cont.

Gd <sub>2</sub> O <sub>3</sub> Content (wt%)	Density (g/cm <sup>3</sup> )		Elemental Composition (% by Weight)			
	Measured	Theoretical	C	O	Si	Gd
10	1.03 ± 0.01	1.02	85.30 ± 2.10	4.39 ± 1.17	0.10 ± 0.09	10.21 ± 1.16
15	1.09 ± 0.01	1.07	80.12 ± 3.31	3.96 ± 0.40	0.13 ± 0.10	15.79 ± 2.87
20	1.12 ± 0.01	1.13	74.51 ± 2.60	5.25 ± 0.27	0.26 ± 0.05	19.98 ± 2.79

### 3.2.2. Thermal Properties of Gd<sub>2</sub>O<sub>3</sub>/r-HDPE Composites

The thermal properties of Gd<sub>2</sub>O<sub>3</sub>/r-HDPE composites with varying Gd<sub>2</sub>O<sub>3</sub> contents (0, 5, 10, 15, and 20 wt%), determined through TGA, are shown in Figure 6. The results reveal that all samples had similar trends in weight loss and thermal stability, as illustrated in Figure 6a, suggesting that the addition of Gd<sub>2</sub>O<sub>3</sub> had little impact on the thermal stability of the r-HDPE composites. In addition, the peaks of the derivative weights (Figure 6b) were in the range 493–495 °C, which corresponds to the decomposition of the r-HDPE matrix [55].



**Figure 6.** Thermal stability of Gd<sub>2</sub>O<sub>3</sub>/r-HDPE composites with varying Gd<sub>2</sub>O<sub>3</sub> contents (0, 5, 10, 15, and 20 wt%), determined through TGA, with (a) correlations between remaining weight of r-HDPE composites and temperature and (b) correlations between derivative weight of r-HDPE composites and temperature.

The percentages of the remaining ash for all samples at 600 °C, derived from Figure 6a, are shown in Table 7, indicating that the amounts of remaining ash were fairly consistent with the nominal contents of the Gd<sub>2</sub>O<sub>3</sub> added to the r-HDPE composites. This behavior was observed mainly due to the Gd<sub>2</sub>O<sub>3</sub> having much higher decomposition temperatures (>600 °C), resulting in the majority of the Gd<sub>2</sub>O<sub>3</sub> particles remaining at 600 °C. The high decomposition temperature of Gd<sub>2</sub>O<sub>3</sub> was confirmed by the TGA results (Figure 7), with less than a 3% loss in the mass of Gd<sub>2</sub>O<sub>3</sub> at 600 °C.

**Table 7.** Remaining ash at 600 °C of Gd<sub>2</sub>O<sub>3</sub>/r-HDPE composites with varying Gd<sub>2</sub>O<sub>3</sub> contents, determined through TGA.

Gd <sub>2</sub> O <sub>3</sub> Content (wt%)	Remaining Ash at 600 °C (%)
0	2.0
5	5.7
10	10.4
15	14.2
20	16.5

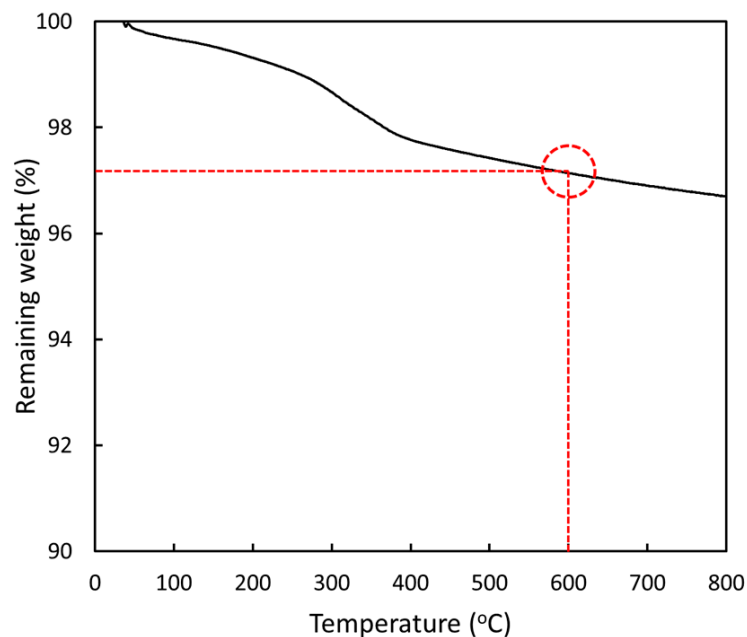


**Figure 7.** Thermal stability of  $\text{Gd}_2\text{O}_3$ , determined through TGA. The dotted circle indicates the remaining weight (%) of  $\text{Gd}_2\text{O}_3$  particles at 600 °C.

### 3.2.3. Crystallinity of $\text{Gd}_2\text{O}_3$ /r-HDPE Composites

The degrees of crystallinity (%XC) for all  $\text{Gd}_2\text{O}_3$ /r-HDPE samples, calculated from the plots of XRD (Figure S1), are shown in Table 8, indicating that the mean ( $\pm$ standard deviation) of %XC abruptly increased with the initial addition of 5 wt%  $\text{Gd}_2\text{O}_3$  into the composites (increase from  $38.6 \pm 4.5\%$  in the pristine r-HDPE to  $53.6 \pm 2.9\%$  in the 5 wt%  $\text{Gd}_2\text{O}_3$ /r-HDPE composites) and then slightly decreased at higher contents. The initial increase in %XC could have been due to the high crystallinity of  $\text{Gd}_2\text{O}_3$  particles that greatly increased the crystalline phase and subsequently increased the overall %XC of the composites. However, as more  $\text{Gd}_2\text{O}_3$  particles were added to the samples, the mobility of the r-HDPE molecular chains was restricted due to the interference of  $\text{Gd}_2\text{O}_3$  particles that retarded the growth in the crystalline phase (hindering the ability of the r-HDPE molecular chains to arrange themselves in an ordered crystalline structure) and subsequently lowered the %XC of the composites [17,56]. It should be noted that the crystalline peaks used for %XC calculations were  $2\theta = 10.3^\circ, 22.4^\circ, 24.8^\circ, 27.6^\circ, 29.4^\circ, 33.9^\circ, 48.2^\circ, \text{ and } 57.3^\circ$ .

**Table 8.** Degrees of crystallinity (%XC) for  $\text{Gd}_2\text{O}_3$ /r-HDPE composites, determined through XRD, with varying  $\text{Gd}_2\text{O}_3$  contents (0, 5, 10, 15, and 20 wt%). The values are shown as the mean  $\pm$  standard deviation of the mean.

$\text{Gd}_2\text{O}_3$ Content (wt%)	Degree of Crystallinity (%)
0	$38.6 \pm 4.5$
5	$53.6 \pm 2.9$
10	$51.4 \pm 4.4$
15	$50.2 \pm 2.5$
20	$50.4 \pm 2.2$

### 3.2.4. Thermal-Neutron-Shielding Properties of $\text{Gd}_2\text{O}_3$ /r-HDPE Composites

The thermal-neutron-shielding properties of non-aged  $\text{Gd}_2\text{O}_3$ /r-HDPE composites with varying  $\text{Gd}_2\text{O}_3$  contents and material thicknesses are shown in Figures 8a and 9. The results indicate that the values of  $I/I_0$ , HVL, and TVL were greatly reduced, while the values of  $\Sigma_t$  and  $\Sigma_{t/\rho}$  increased, when 5 wt% of  $\text{Gd}_2\text{O}_3$  was initially introduced to the composites. For example, the values of  $I/I_0$  and HVL decreased from 0.98 and

5.38 cm, respectively, in the 2 mm r-HDPE sample to 0.41 and 0.16 cm, respectively, in the 2 mm r-HDPE sample containing 5 wt% Gd<sub>2</sub>O<sub>3</sub>, corresponding to an approximately 34-fold reduction in the materials needed to attenuate 50% of the initial neutron intensity. This pronounced improvement in the ability of the composites to attenuate thermal neutrons was primarily attributed to a shift in dominant neutron interactions from neutron scattering in the pristine r-HDPE sample to a more effective mechanism of neutron absorption in the Gd<sub>2</sub>O<sub>3</sub>/r-HDPE composites, due to the presence of Gd elements with a high value of  $\sigma_{\text{abs}}$  [57], consequently leading to the enhanced probability of thermal neutrons being absorbed by the Gd<sub>2</sub>O<sub>3</sub>/r-HDPE composites. Figures 8a and 9 also show that by adding more Gd<sub>2</sub>O<sub>3</sub> particles to the composites, the improvement in the shielding abilities of the composites became less pronounced, especially at higher (>15 wt%) Gd<sub>2</sub>O<sub>3</sub> contents. This observed result could have been due to the existence of the neutron absorption mechanism at 5 wt% content, resulting in just a slight additional probability for thermal neutrons to be absorbed by the added Gd<sub>2</sub>O<sub>3</sub> particles. Another possible explanation for this small improvement could be that the particle agglomeration and non-uniformity of the Gd distribution in the matrix (Figure 10), especially in the samples with high Gd<sub>2</sub>O<sub>3</sub> contents (Figure 10c,d), limited the capability of the Gd elements to interact with neutrons [58]. Furthermore, Figure 8a reveals negative correlations between  $I/I_0$  and material thickness ( $x$ ); hence, the ability of the samples to attenuate neutrons increased with increasing material thickness. This was observed primarily because there were a greater number of Gd elements per unit area of the sample that could interact and attenuate neutrons. In fact, this correlation was in agreement with the Beer–Lambert equation (Equation (3)) [59], which also depicts a negative relationship between  $I/I_0$  and  $x$  [37]:

$$I/I_0 = e^{-\Sigma_t \cdot x} \quad (3)$$

Figures 8b and 9 illustrate the thermal-neutron-shielding properties of the Gd<sub>2</sub>O<sub>3</sub>/r-HDPE composites after being gamma irradiated with a total dose of 70 kGy. The results indicate that there were slight decreases in the overall shielding properties of the gamma-aged samples, which might have been due to the initiation of chain scission and oxidative degradation caused by the gamma rays that altered the molecular structures and physical properties of the composites [60], resulting in more neutrons being able to transmit through the materials, leading to higher values for  $I/I_0$ , HVL, and TVL (lower values for  $\Sigma_t$  and  $\Sigma_t/\rho$ ).

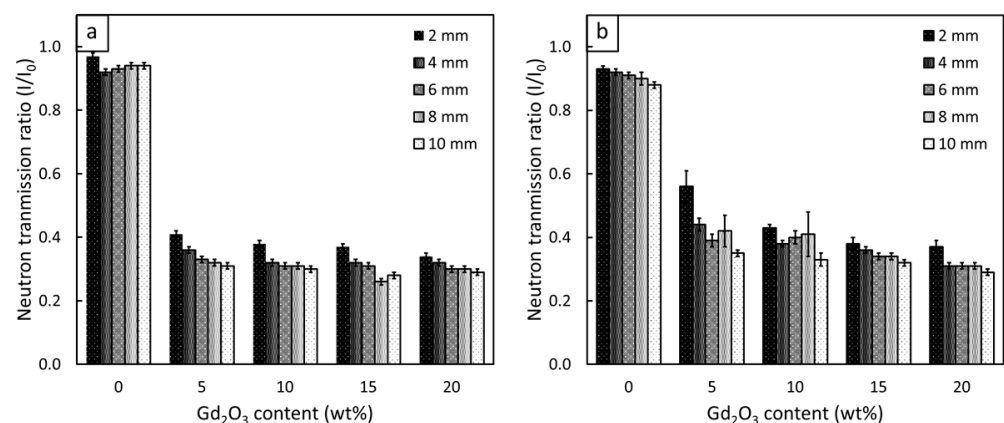


**Figure 8.** Neutron transmission ratios of (a) non-aged Gd<sub>2</sub>O<sub>3</sub>/r-HDPE composites and (b) gamma-aged Gd<sub>2</sub>O<sub>3</sub>/r-HDPE composites, with varying Gd<sub>2</sub>O<sub>3</sub> contents and sample thicknesses, where error bars indicate  $\pm$  standard deviation.

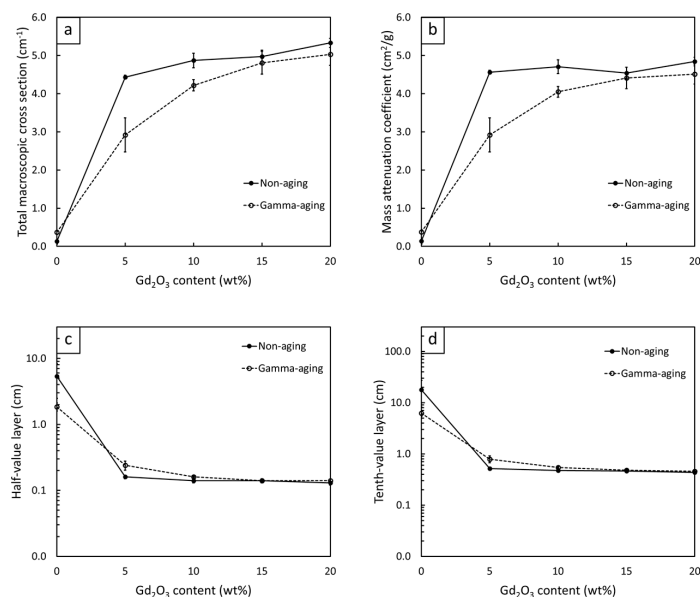


**Figure 9.** Thermal-neutron-shielding properties, consisting of (a) total macroscopic cross section ( $\Sigma_t$ ), (b) mass attenuation coefficient ( $\Sigma_t/\rho$ ), (c) half-value layer (HVL), and (d) tenth value layer (TVL) of non-aged  $\text{Gd}_2\text{O}_3/\text{r-HDPE}$  composites (solid lines) and gamma-aged  $\text{Gd}_2\text{O}_3/\text{r-HDPE}$  composites (dotted lines), where error bars indicate  $\pm$  standard deviation.

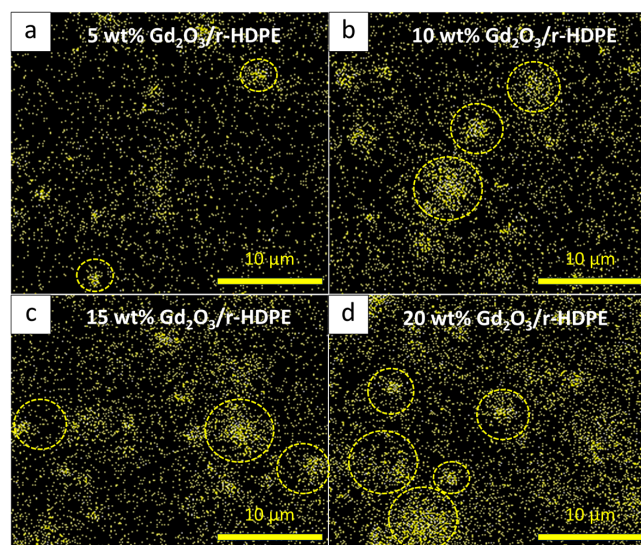


**Figure 10.** SEM-EDX mapping of Gd distribution in  $\text{Gd}_2\text{O}_3/\text{r-HDPE}$  composites with varying  $\text{Gd}_2\text{O}_3$  contents of (a) 5 wt%, (b) 10 wt%, (c) 15 wt%, and (d) 20 wt%. Dotted circles indicate areas with visible Gd agglomeration.

### 3.2.5. Mechanical Properties of $\text{Gd}_2\text{O}_3/\text{r-HDPE}$ Composites

Figure 11 shows the mechanical properties, consisting of tensile modulus, tensile strength, elongation at break, and hardness (Shore D), of the non-aged and gamma-aged  $\text{Gd}_2\text{O}_3/\text{r-HDPE}$  composites with varying  $\text{Gd}_2\text{O}_3$  contents (0, 5, 10, 15, and 20 wt%). The results indicate that the hardness (Shore D) gradually increased after the addition of  $\text{Gd}_2\text{O}_3$ , with the values rising up to  $63 \pm 1$  for the sample containing 20 wt%  $\text{Gd}_2\text{O}_3$  (compared to  $55 \pm 3$  for the neat r-HDPE sample). The increase in hardness (Shore D) could have been due to the high rigidity of the  $\text{Gd}_2\text{O}_3$  particles that subsequently increased the overall rigidity and hence the surface hardness of the composites [23]. Notably, the behaviors of tensile modulus and surface hardness for the samples with varying  $\text{Gd}_2\text{O}_3$  contents were similar to those of the crystallinity shown in Table 8, which could be due to the crystalline

regions within the sample tending to be more ordered and densely packed than those of amorphous regions, resulting in the samples with higher %XD exhibiting greater resistance to deformation and, hence, higher overall rigidity. On the other hand, the values of tensile modulus, tensile strength, and elongation at break behaved differently, with the values of tensile modulus/tensile strength increasing up to 15 wt% of  $Gd_2O_3$  and elongation at break increasing up to 5 wt% of  $Gd_2O_3$ , and then gradually decreasing at higher  $Gd_2O_3$  contents. These initial increases in the mentioned tensile properties could have been due to the improved filler dispersion within the r-HDPE matrix from the additional surface treatment, which subsequently improved the filler–matrix bonding at their interfaces and, subsequently, the abilities to transfer external forces from the matrix to the fillers [17]. However, as more  $Gd_2O_3$  particles were added to the composites, there was noticeably higher particle agglomeration due to filler–filler interactions [61], as well as visible voids from the interfacial incompatibility between the  $Gd_2O_3$  particles and the r-HDPE matrix (despite  $Gd_2O_3$  being treated with KBE903) [62], resulting in the limited mobility of the r-HDPE molecular chains that restricted the deformation of the composites [17]. Micrographs illustrating the morphologies and particle distribution of all samples are shown in Figure 12, which reveals visible voids and agglomerations in the materials, especially in those with high filler contents (Figure 12d,e).

In addition, Figure 11 shows the changes in the mechanical properties of the  $Gd_2O_3$ /r-HDPE composites after being gamma irradiated (gamma aging). The results indicate that the tensile modulus values mostly increased after aging, which could have been due to the initiation of additional crosslinking between the r-HDPE molecular chains by gamma rays, which increased the overall rigidity and hence the tensile modulus of the composites [63]. Nonetheless, the values for tensile strength, elongation at break, and hardness (Shore D) for the non-aged and gamma-aged samples were not significantly different, except for the sample containing 5 wt%  $Gd_2O_3$ , which had a noticeable reduction in elongation at break after aging. The small changes in the tensile properties could have been due to the high atomic number of Gd, as well as the relatively high density of  $Gd_2O_3$ , which made  $Gd_2O_3$  interact well with incoming gamma rays and subsequently suppress the effects of chain scission and oxidative degradation that would normally reduce the mechanical properties of the materials [27,64,65]. However, as previously mentioned, the elongation at break of the gamma-aged  $Gd_2O_3$ /r-HDPE composites with 5 wt% of  $Gd_2O_3$  was significantly lower than that of the non-aged one. This could have been due to insufficient  $Gd_2O_3$  content to suppress the degradation (chain scission) caused by gamma rays, resulting in reduced abilities of the composites to elongate along the direction of external forces.

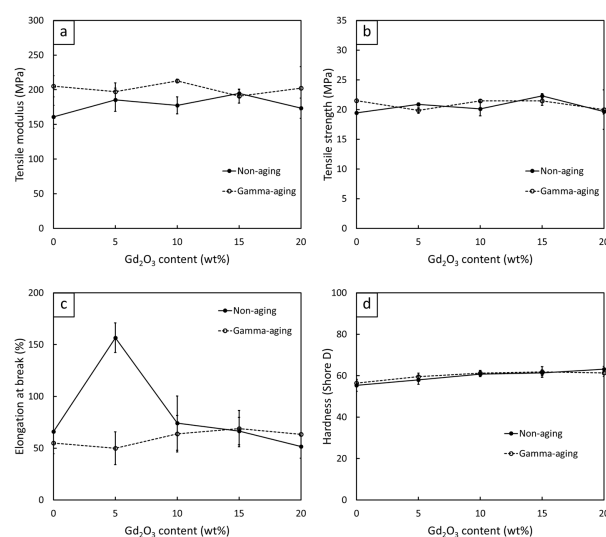


**Figure 11.** Mechanical properties, consisting of (a) tensile modulus, (b) tensile strength, (c) elongation at break, and (d) hardness (Shore D) of non-aged  $Gd_2O_3$ /r-HDPE composites (solid lines) and gamma-aged  $Gd_2O_3$ /r-HDPE composites (dotted lines), where error bars indicate  $\pm$  standard deviation.

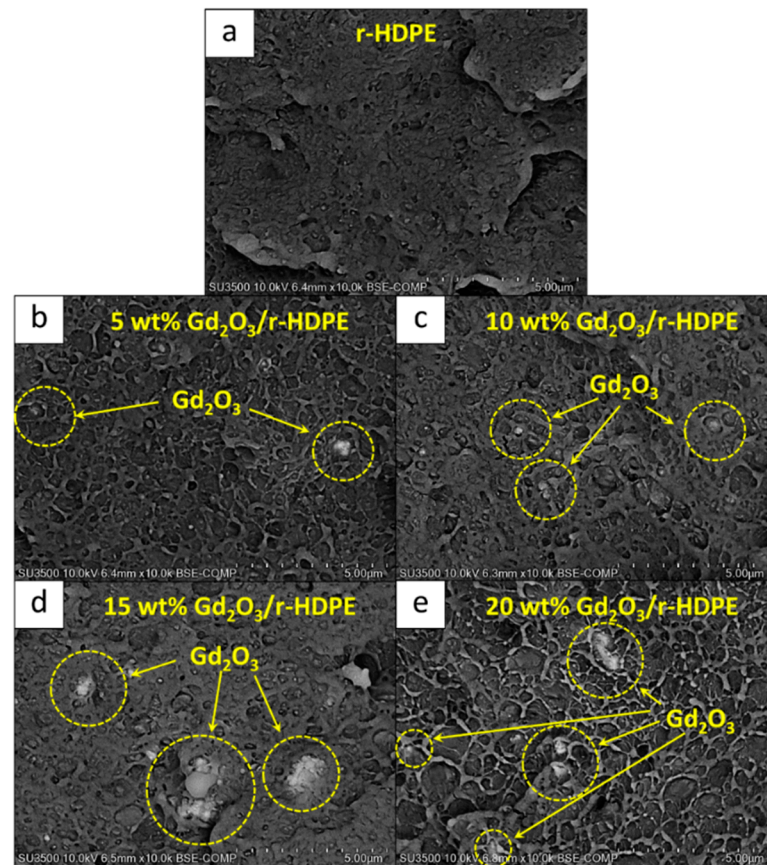


**Figure 12.** SEM images showing morphologies and particle distributions in (a) a pristine r-HDPE, and Gd<sub>2</sub>O<sub>3</sub>/r-HDPE composites with varying Gd<sub>2</sub>O<sub>3</sub> contents of (b) 5 wt%, (c) 10 wt%, (d) 15 wt%, and (e) 20 wt%. Dotted circles indicate areas with visible particle agglomeration.

### 3.3. Benchmarking Developed r-HDPE Composites with Commercial Borated Polyethylene (PE) Products

To determine the useability and to benchmark the developed r-HDPE composites, their thermal-neutron-shielding and mechanical properties were compared with those from commonly used neutron-shielding products based on borated PE composites that contain 5 wt% and 15 wt% of boron (B), as shown in Table 9. The results indicate that the overall thermal-neutron-shielding properties of the 5 wt% Gd<sub>2</sub>O<sub>3</sub>/r-HDPE composites had much higher values than those of the borated PE products (for both boron contents), as evidenced by the higher values of  $\Sigma_t$  and  $\Sigma_{t/\rho}$  and the lower values of HVL and TVL in the former. These substantially improved shielding properties could have been due to the much higher  $\sigma_{\text{abs}}$  value of Gd (49,700 barns) than that of B (767 barns) [25], resulting in a higher interaction probability between neutrons and Gd<sub>2</sub>O<sub>3</sub> particles. Table 9 also shows that the commercial products were noticeably more brittle than the current r-HDPE composites, as seen in the lower tensile strength (as low as 16.6 MPa) and elongation at break (as low as 4%) in the former. The brittleness observed in the commercial products could have been due to the lower densities of boron compounds, such as boron carbide (2.52 g/cm<sup>3</sup>) or boron oxide (2.46 g/cm<sup>3</sup>), which led to an increased volume of fillers being added to the matrix to obtain the required boron contents, resulting in potentially more defects or particle agglomerations, or both, being observed in the matrix, which subsequently lowered the values of the tensile strength and elongation at break of the products.

**Table 9.** Comparative thermal-neutron-shielding and mechanical properties of 5 wt% Gd<sub>2</sub>O<sub>3</sub>/r-HDPE composites in this work and commercial PE products containing 5 wt% and 15 wt% of boron (B).

Property	5 wt% Gd <sub>2</sub> O <sub>3</sub> /r-HDPE	Borated PE **		Standard of Testing
		5 wt%	15 wt%	
Thermal-neutron-shielding properties *				
Total macroscopic cross section (cm <sup>-1</sup> )	4.43	0.36	0.60	–
Mass attenuation coefficient (cm <sup>2</sup> /g)	4.56	0.41	0.57	–
Half-value layer (cm)	0.16	1.94	1.15	–
Tenth value layer (cm)	0.52	6.43	3.80	–
Mechanical properties				
Tensile modulus (MPa)	185.5	>700	766.7	ASTM D638
Tensile strength (MPa)	20.9	>20	16.6	ASTM D638
Elongation at break (%)	157	–	4	ASTM D638
Hardness (Shore D)	60	>63	70	ASTM D2240

\* Thermal neutron shielding measurements were carried out according to the procedure described in Section 2.4.1.

\*\* The mechanical properties of borated PE products were obtained from provided specifications in their respective datasheets.

As mentioned above, based on the overall comparisons between the developed 5 wt% Gd<sub>2</sub>O<sub>3</sub>/r-HDPE composites in this work and commercial PE products containing 5 wt% and 15 wt% of boron (B), it was evident that the r-HDPE composites had promising potential as effective thermal-neutron-shielding materials by offering highly efficient neutron attenuation as well as enhanced mechanical properties that widened the possible usage and application of the composites.

#### 4. Conclusions

This research addressed the increasing demand for enhanced radiation safety and environmental concerns whilst addressing concerns about increasing plastic pollution by developing efficient and eco-friendly thermal-neutron-shielding materials using r-HDPE composites with varying contents of silane-treated Gd<sub>2</sub>O<sub>3</sub>. The results demonstrate that the addition of Gd<sub>2</sub>O<sub>3</sub> significantly improved the thermal-neutron-shielding capabilities of the r-HDPE composites, as seen in the lower values for I/I<sub>0</sub>, HVL, and TVL and higher values of  $\Sigma_t$  and  $\Sigma_{t/\rho}$  after the addition of Gd<sub>2</sub>O<sub>3</sub>. Additionally, the mechanical properties, consisting of tensile modulus, tensile strength, and elongation at break, were initially enhanced with the addition of up to 5–15 wt% of Gd<sub>2</sub>O<sub>3</sub>, and then gradually declined at higher contents. Furthermore, the addition of Gd<sub>2</sub>O<sub>3</sub> increased the values for surface hardness (Shore D),  $\rho$ , remaining ash at 600 °C, and the %XC of the composites. This study also investigated the impact of gamma irradiation on these composites, revealing a slight increase in tensile modulus, while tensile strength, elongation at break, and hardness (Shore D) remained relatively unaffected, except for in the 5 wt% Gd<sub>2</sub>O<sub>3</sub> sample, which experienced a significant reduction in elongation at break. Furthermore, in comparing these r-HDPE composites with conventional neutron-shielding products based on PE composites containing 5 wt% and 15 wt% boron, our findings indicate that the r-HDPE composites had superior shielding and tensile properties than the latter, highlighting the potential of r-HDPE composites to replace virgin plastics as effective and more environmentally friendly shielding materials. Consequently, based on the overall results obtained, the developed r-HDPE composites could be used as alternative materials that not only offer highly effective thermal-neutron-shielding capability, but also provide a basis for the future development of high-valued recycled products.

**Supplementary Materials:** The following are available online at <https://www.mdpi.com/article/10.3390/polym16081139/s1>: Figure S1: XRD spectra of Gd<sub>2</sub>O<sub>3</sub>/r-HDPE composites containing varying Gd<sub>2</sub>O<sub>3</sub> contents of 0–20 wt%. The dotted red lines represent peak positions used for the calculation of crystallinity.

**Author Contributions:** Conceptualization, K.S.; formal analysis, D.T., E.W., K.H., P.L. and K.S.; funding acquisition, D.T. and K.S.; investigation, D.T., E.W., K.H., P.L. and K.S.; methodology, D.T., E.W., K.H., P.L. and K.S.; supervision, K.S.; validation, D.T., E.W., K.H., P.L. and K.S.; visualization, K.S.; writing—original draft K.S.; writing—review and editing, D.T., E.W., K.H., P.L. and K.S. All authors have read and agreed to the published version of the manuscript.

**Funding:** This research was financially supported by the Kasetsart University Research and Development Institute (KURDI), Bangkok, Thailand, grant number FF(KU)51.67; the Thailand Institute of Nuclear Technology (Public Organization), Nakhorn Nayok, Thailand; and the National Research Council of Thailand (NRCT), grant number N41A650069.

**Data Availability Statement:** Data will be made available on request (due to privacy).

**Acknowledgments:** The Specialized Center of Rubber and Polymer Materials in Agriculture and Industry (RPM) provided publication support, and the Polymer Processing and Flow (P-PROF) Research Group, King Mongkut's University of Technology Thonburi, and the Office of Atoms for Peace (OAP) provided equipment and laboratory support.

**Conflicts of Interest:** The authors declare that they have no known competing financial interests or personal relationships that could appear to influence the work reported in this paper.

## References

1. Kardjilov, N.; Manke, I.; Hilger, A.; Strobl, M.; Banhart, J. Neutron imaging in materials science. *Mater. Today* **2011**, *14*, 248–256. [[CrossRef](#)]
2. Kardjilov, N.; Manke, I.; Woracek, R.; Hilger, A.; Banhart, J. Advances in neutron imaging. *Mater. Today* **2018**, *21*, 652–672. [[CrossRef](#)]
3. Moss, R.L. Critical review, with an optimistic outlook, on Boron Neutron Capture Therapy (BNCT). *Appl. Radiat. Isot.* **2014**, *88*, 2–11. [[CrossRef](#)]
4. Ohta, M.; Kwon, S.; Sato, S.; Ochiai, K.; Suzuki, H. Investigation of Mo-99 radioisotope production by d-Li neutron source. *Nucl. Mater. Energy* **2018**, *15*, 261–266. [[CrossRef](#)]
5. Meier, W.R.; Abbott, R.; Beach, R.; Bink, J.; Caird, J.; Erlandson, A.; Farmer, J.; Halsey, W.; Ladran, T.; Latkowski, J.; et al. Systems modeling for the Laser Fusion-Fission Energy (LIFE) power plant. *Fusion Sci. Technol.* **2009**, *56*, 647–651. [[CrossRef](#)]
6. Bustreo, C.; Giuliani, U.; Maggio, D.; Zollino, G. How fusion power can contribute to a fully decarbonized European power mix after 2050. *Fusion Eng. Des.* **2019**, *146*, 2189–2193. [[CrossRef](#)]
7. Channuie, J.; Sinkaew, P.; Lekchaum, S.; Kanjana, K. In-house development of neutron moisture gauge for field measurement. *J. Phys. Conf. Ser.* **2017**, *901*, 012148. [[CrossRef](#)]
8. Timakova, R.T.; Iliukhin, R.V.; Iliukhina, V. Modern trends in the development of nuclear power: From environmental friendliness to safe utilitarianism. *IOP Conf. Ser. Earth Environ. Sci.* **2022**, *979*, 012172. [[CrossRef](#)]
9. Lomax, M.E.; Folkes, L.K.; O'Neill, P. Biological consequences of radiation-induced DNA damage: Relevance to radiotherapy. *Clin. Oncol.* **2013**, *25*, 578–585. [[CrossRef](#)]
10. Reisz, J.A.; Bansal, N.; Qian, J.; Zhao, W.; Furdui, C.M. Effects of ionizing radiation on biological molecules—Mechanisms of damage and emerging methods of detection. *Antioxid. Redox Signal.* **2014**, *21*, 260–292. [[CrossRef](#)]
11. Chambers, C.E.; Fetterly, K.; Holzer, R.; Lin, P.P.; Blankenship, J.C.; Balter, S.; Laskey, W.K. Radiation safety program for the cardiac catheterization laboratory. *Catheter. Cardiovasc. Interv.* **2011**, *77*, 546–556. [[CrossRef](#)]
12. Gellis, L.A.; Ceresnak, S.R.; Gates, G.J.; Nappo, L.; Pass, R.H. Reducing patient radiation dosage during pediatric SVT ablations using an “ALARA” radiation reduction protocol in the modern fluoroscopic era. *Pacing Clin. Electrophysiol.* **2013**, *36*, 688–694. [[CrossRef](#)]
13. Poltabtim, W.; Wimolmala, E.; Markpin, T.; Sombatsompop, N.; Rosarpitak, V.; Saenboonruang, K. X-ray shielding, mechanical, physical, and water absorption properties of wood/PVC composites containing bismuth oxide. *Polymers* **2021**, *13*, 2212. [[CrossRef](#)] [[PubMed](#)]
14. Ozdemir, T.; Akbay, I.K.; Uzun, H.; Reyhancan, I.A. Neutron shielding of EPDM rubber with boric acid: Mechanical, thermal properties and neutron absorption tests. *Prog. Nucl. Energy* **2016**, *89*, 102–109. [[CrossRef](#)]
15. Toyen, D.; Saenboonruang, K. Development of paraffin and paraffin/bitumen composites with additions of B<sub>2</sub>O<sub>3</sub> for thermal neutron shielding applications. *J. Nucl. Sci. Technol.* **2017**, *54*, 871–877. [[CrossRef](#)]
16. Zhang, X.; Yang, M.; Zhang, X.; Wu, H.; Guo, S.; Wang, Y. Enhancing the neutron shielding ability of polyethylene composites with an alternating multi-layered structure. *Compos. Sci. Technol.* **2017**, *150*, 16–23. [[CrossRef](#)]
17. Toyen, D.; Anekramontre, T.; Wimolmala, E.; Thamrongsiripak, N.; Rungseesumran, T.; Saenboonruang, K. Comparisons of enhanced thermal neutron- and gamma-shielding properties in UHMWPE composites containing surface-treated Sm<sub>2</sub>O<sub>3</sub> and Gd<sub>2</sub>O<sub>3</sub> particles. *Polym. Adv. Technol.* **2023**, *34*, 2394–2406. [[CrossRef](#)]
18. Kharita, M.H.; Yousef, S.; Al Nassar, M. Review on the addition of boron compounds to radiation shielding concrete. *Prog. Nucl. Energy* **2011**, *53*, 207–211. [[CrossRef](#)]
19. Ozdemir, T.; Gungor, A.; Reyhancan, I.A. Flexible neutron shielding composite material of EPDM rubber with boron trioxide: Mechanical, thermal investigations and neutron shielding tests. *Radiat. Phys. Chem.* **2017**, *131*, 7–12. [[CrossRef](#)]
20. Uddin, Z.; Yasin, T.; Shafiq, M.; Raza, A.; Zahur, A. On the physical, chemical, and neutron shielding properties of polyethylene/boron carbide composites. *Radiat. Phys. Chem.* **2020**, *166*, 108450. [[CrossRef](#)]

21. Shang, Y.; Yang, G.; Su, F.; Feng, Y.; Ji, Y.; Liu, D.; Yin, R.; Liu, C.; Shen, C. Multilayer polyethylene/hexagonal boron nitride composites showing high neutron shielding efficiency and thermal conductivity. *Compos. Commun.* **2020**, *19*, 147–153. [[CrossRef](#)]
22. Zhang, W.; Feng, Y.; Althakafy, J.T.; Liu, Y.; Abo-Dief, H.M.; Huang, M.; Zhou, L.; Su, F.; Liu, C.; Shen, C. Ultrahigh molecular weight polyethylene fiber/boron nitride composites with high neutron shielding efficiency and mechanical performance. *Adv. Compos. Hybrid Mater.* **2022**, *5*, 2012–2020. [[CrossRef](#)]
23. Ninyong, K.; Wimolmala, E.; Sombatsompop, N.; Saenboonruang, K. Potential use of NR and wood/NR composites as thermal neutron shielding materials. *Polym. Test.* **2017**, *59*, 336–343. [[CrossRef](#)]
24. Ninyong, K.; Wimolmala, E.; Sombatsompop, N.; Saenboonruang, K. Properties of natural rubber (NR) and wood/NR composites as gamma shielding materials. *IOP Conf. Ser. Mater. Sci. Eng.* **2018**, *526*, 012038. [[CrossRef](#)]
25. Dumazert, J.; Coulon, R.; Lecomte, Q.; Bertrand, G.H.V.; Hamel, M. Gadolinium for neutron detection in current nuclear instrumentation research: A review. *Nucl. Instrum. Methods Phys. Res. A* **2018**, *882*, 53–68. [[CrossRef](#)]
26. Castley, D.; Goodwin, C.; Liu, J. Computational and experimental comparison of boron carbide, gadolinium oxide, samarium oxide, and graphene platelets as additives for a neutron shield. *Radiat. Phys. Chem.* **2019**, *165*, 108435. [[CrossRef](#)]
27. Saenboonruang, K.; Poltabtim, W.; Thumwong, A.; Pianpanit, T.; Rattanapongs, C. Rare-earth oxides as alternative high-energy photon protective fillers in HDPE composites: Theoretical aspects. *Polymers* **2021**, *13*, 1930. [[CrossRef](#)]
28. Saleh, A. Comparative shielding features for X/Gamma-rays, fast and thermal neutrons of some gadolinium silicoborate glasses. *Prog. Nucl. Energy* **2022**, *154*, 104482. [[CrossRef](#)]
29. Poltabtim, W.; Thumwong, A.; Wimolmala, E.; Rattanapongs, C.; Tokonami, S.; Ishikawa, T.; Saenboonruang, K. Dual X-ray- and neutron-shielding properties of Gd<sub>2</sub>O<sub>3</sub>/NR composites with autonomous self-healing capabilities. *Polymers* **2022**, *14*, 4481. [[CrossRef](#)]
30. Nguyen, K.Q.; Mwiseneza, C.; Mohamed, K.; Cousin, P.; Robert, M.; Benmokrane, B. Long-term testing methods for HDPE pipe-advantages and disadvantages: A review. *Eng. Fract. Mech.* **2021**, *246*, 107629. [[CrossRef](#)]
31. Lavelle, C.M.; Liu, C.Y.; Stone, M.B. Toward a new polyethylene scattering law determined using inelastic neutron scattering. *Nucl. Instrum. Methods Phys. Res. A* **2013**, *711*, 166–179. [[CrossRef](#)]
32. Khaleel, R.; Valsan, G.; Rangel-Buitrago, N.; Warrior, A.K. Hidden problems in geological heritage sites: The microplastic issue on Saint Mary's Island, India, Southeast Arabian Sea. *Mar. Pollut. Bull.* **2022**, *182*, 114043. [[CrossRef](#)]
33. Achilias, D.S.; Roupakias, C.; Megalokonomos, P.; Lappas, A.A.; Antonakou, E.V. Chemical recycling of plastic wastes made from polyethylene (LDPE and HDPE) and polypropylene (PP). *J. Hazard. Mater.* **2007**, *149*, 536–542. [[CrossRef](#)] [[PubMed](#)]
34. Xia, C.; Han, B. Plastics upcycling made more sustainable and practical. *Nat. Sustain.* **2023**, *6*, 1518–1519. [[CrossRef](#)]
35. Mahmoud, M.E.; El-Khatib, A.M.; Badawi, M.S.; Rashad, A.R.; El-Sharkawy, R.M.; Thabet, A.A. Recycled high-density polyethylene plastics added with lead oxide nanoparticles as sustainable radiation shielding materials. *J. Clean. Prod.* **2018**, *176*, 276–287. [[CrossRef](#)]
36. King, M.F.; Gutberlet, J. Contribution of cooperative sector recycling to greenhouse gas emissions reduction: A case study of Ribeirão Pires, Brazil. *Waste Manag.* **2013**, *33*, 2771–2780. [[CrossRef](#)] [[PubMed](#)]
37. Toyen, D.; Paopun, Y.; Changjan, D.; Wimolmala, E.; Mahathanabodee, S.; Pianpanit, T.; Anekratmontree, T.; Saenboonruang, K. Simulation of neutron/self-emitted gamma attenuation and effects of silane surface treatment on mechanical and wear resistance properties of Sm<sub>2</sub>O<sub>3</sub>/UHMWPE composites. *Polymers* **2021**, *13*, 3390. [[CrossRef](#)] [[PubMed](#)]
38. Toyen, D.; Wimolmala, E.; Sombatsompop, N.; Saenboonruang, K. Sm<sub>2</sub>O<sub>3</sub>/UHMWPE composites for radiation shielding applications: Mechanical and dielectric properties under gamma irradiation and thermal neutron shielding. *Radiat. Phys. Chem.* **2019**, *164*, 108366. [[CrossRef](#)]
39. Kires, M. Archimedes' principle in action. *Phys. Educ.* **2007**, *42*, 484. [[CrossRef](#)]
40. ASTM D792-13; Standard Test Methods for Density and Specific Gravity (Relative Density) of Plastics by Displacement. ASTM International: West Conshohocken, PA, USA, 2013.
41. Moonart, U.; Utara, S. Effect of surface treatments and filler loading on the properties of hemp fiber/natural rubber composites. *Cellulose* **2019**, *26*, 7271–7295. [[CrossRef](#)]
42. Lopez-Rubio, A.; Flanagan, B.M.; Gilbert, E.P.; Gidley, M.J. A novel approach for calculating starch crystallinity and its correlation with double helix content: A combined XRD and NMR study. *BioPolymers* **2008**, *89*, 761–768. [[CrossRef](#)] [[PubMed](#)]
43. ASTM D638-14; Standard Test Method for Tensile Properties of Plastics (Metric). ASTM International: West Conshohocken, PA, USA, 2014.
44. ASTM D2240-03; Standard Test Method for Rubber Property-Durometer Hardness. ASTM International: West Conshohocken, PA, USA, 2003.
45. Issa, A.A.; Luyt, A.S. Kinetics of alkoxysilanes and organoalkoxysilanes polymerization: A review. *Polymers* **2019**, *11*, 537. [[CrossRef](#)] [[PubMed](#)]
46. Ataabadi, M.R.; Jamshidi, M. Silane modification of TiO<sub>2</sub> nanoparticles and usage in acrylic film for effective photocatalytic degradation of methylene blue under visible light. *Sci. Rep.* **2023**, *13*, 7383. [[CrossRef](#)] [[PubMed](#)]
47. Liu, X.; Chen, X.; Ren, J.; Zhang, C. TiO<sub>2</sub>-KH550 nanoparticle-reinforced PVA/xylan composite films with multifunctional properties. *Materials* **2018**, *11*, 1589. [[CrossRef](#)] [[PubMed](#)]
48. Pantoja, M.; Diaz-Benito, B.; Velasco, F.; Abenojar, A.; del Real, J.C. Analysis of hydrolysis process of  $\gamma$ -methacryloxypropyltrimethoxysilane and its influence on the formation of silane coatings on 6063 aluminum alloy. *Appl. Surf. Sci.* **2009**, *255*, 6386–6390. [[CrossRef](#)]
49. Sae-Oui, P.; Sirisinha, C.; Thepsuwan, U.; Hatthapanit, K. Roles of silane coupling agents on properties of silica-filled polychloroprene. *Eur. Polym. J.* **2006**, *42*, 479–486. [[CrossRef](#)]
50. Zanchi, C.H.; Ogliari, F.A.; Silva, R.M.; Lund, R.G.; Machado, H.H.; Prati, C.; Carreno, N.L.V.; Piva, E. Effect of the silane concentration on the selected properties of an experimental microfilled composite resin. *Appl. Adhes. Sci.* **2015**, *3*, 27. [[CrossRef](#)]

51. Xie, Y.; Hill, C.A.S.; Xiao, Z.; Militz, H.; Mai, C. Silane coupling agents used for natural fiber/polymer composites: A review. *Compos. A Appl. Sci. Manuf.* **2010**, *41*, 806–819. [[CrossRef](#)]
52. Yang, H.S.; Wolcott, M.P.; Kim, H.S.; Kim, S.; Kim, H.J. Effect of different compatibilizing agents on the mechanical properties of lignocellulosic material filled polyethylene bio-composites. *Compos. Struct.* **2007**, *79*, 369–375. [[CrossRef](#)]
53. Gao, X.; Lin, L.; Pang, J.; Chen, F.; Li, Q. Effects of impulse-cyclone drying and silane modification on the properties of wood fiber/HDPE composite material. *Carbohydr. Polym.* **2019**, *207*, 343–351. [[CrossRef](#)]
54. Taheraslani, M.; Gardeniers, H. High-resolution SEM and EDX characterization of deposits formed by CH<sub>4</sub>+Ar DBD plasma processing in a packed bed reactor. *Nanomaterials* **2019**, *9*, 589. [[CrossRef](#)] [[PubMed](#)]
55. Aigbodion, V.S.; Hassan, S.B.; Atuanya, C.U. Kinetics of isothermal degradation studies by thermogravimetric data: Effect of orange peels ash on thermal properties of high density polyethylene (HDPE). *J. Mater. Environ. Sci.* **2012**, *3*, 1027–1036.
56. Bornani, K.; Rahman, M.A.; Benicewicz, B.; Kumar, S.; Schadler, L. Using nanofiller assemblies to control the crystallization kinetics of high-density polyethylene. *Macromolecules* **2021**, *54*, 5673–5682. [[CrossRef](#)]
57. Ho, S.L.; Yue, H.; Tegafaw, T.; Ahmad, M.Y.; Liu, S.; Nam, S.W.; Chang, Y.; Lee, G.H. Gadolinium Neutron Capture Therapy (GdNCT) agents from molecular to nano: Current status and perspectives. *ACS Omega* **2022**, *7*, 2533–2553. [[CrossRef](#)] [[PubMed](#)]
58. Zhai, H.; Zhong, S.; Li, J.; Chen, Y.; Cui, Y.; Chen, Z.; Sun, G.; Wang, H. The neutron shielding modeling and experimental characteristic in TiB<sub>2</sub>/Al composites. *Mater. Today Commun.* **2021**, *27*, 102194. [[CrossRef](#)]
59. Malidarre, R.B.; Akkurt, I.; Zakaly, H.M.H. Investigation of Ag as chemical modifier in glassy SeTe chalcogenide alloy in terms of radiation shielding, optical, structural, and physical properties. *Radiat. Phys. Chem.* **2023**, *204*, 110685. [[CrossRef](#)]
60. Alsabbagh, A.; Saleem, R.A.; Almasri, R.; Aljarrah, S.; Awad, S. Effects of gamma irradiation on 3D-printed polylactic acid (PLA) and high-density polyethylene (HDPE). *Polym. Bull.* **2021**, *78*, 4931–4945. [[CrossRef](#)]
61. Nandi, S.; Bose, S.; Mitra, S.; Ghosh, A.K. Dynamic rheology and morphology of HDPE-fumed silica composites: Effect of interface modification. *Polym. Eng. Sci.* **2013**, *53*, 644–650. [[CrossRef](#)]
62. Wang, X.; Yu, Z.; McDonald, A.G. Effect of different reinforcing fillers on properties, interfacial compatibility and weatherability of wood-plastic composites. *J. Bionic Eng.* **2019**, *16*, 337–353. [[CrossRef](#)]
63. Martinez-Morlanes, M.J.; Castell, P.; Martinez-Nogues, V.; Martinez, M.T.; Alonso, P.J.; Puertolas, J.A. Effects of gamma-irradiation on UHMWPE/MWNT nanocomposites. *Compos. Sci. Technol.* **2011**, *71*, 282–288. [[CrossRef](#)]
64. Otaguro, H.; de Lima, L.F.C.P.; Parra, D.F.; Lugao, A.B.; Chinelatto, M.A.; Canevarolo, S.V. High-energy radiation forming chain scission and branching in polypropylene. *Radiat. Phys. Chem.* **2010**, *79*, 318–324. [[CrossRef](#)]
65. Chaiphaksa, W.; Borisut, P.; Chantima, N.; Kaewkhao, J.; Sanwaranatee, N.W. Mathematical calculation of gamma rays interaction in bismuth gadolinium silicate glass using WinXCom program. *Mater. Today Proc.* **2022**, *65*, 2412–2415. [[CrossRef](#)]

**Disclaimer/Publisher’s Note:** The statements, opinions and data contained in all publications are solely those of the individual author(s) and contributor(s) and not of MDPI and/or the editor(s). MDPI and/or the editor(s) disclaim responsibility for any injury to people or property resulting from any ideas, methods, instructions or products referred to in the content.